Available online at www.sciencedirect.com
SCIENCE DIRECT®

Journal of the European Ceramic Society 23 (2003) 595–602

www.elsevier.com/locate/jeurceramsoc

Corrosion of silicon nitride in aqueous acidic solutions: penetration monitoring

B. Seipel, K.G. Nickel*

Applied Mineralogy, Faculty of Geoscience, University of Tuebingen, Germany

Received 4 October 2001; received in revised form 5 August 2002; accepted 8 August 2002

Abstract

The degradation behaviour of silicon nitride in aqueous acidic solutions under steady state conditions was studied at 90 °C and different flow rates. Two different compositions were chosen: Si_3N_4 + 4 wt.% Al_2O_3 + 6% Y_2O_3 (SN0) and Si_3N_4 + 2.4 wt.% $MgAl_2O_4$ + 1.3 wt.% Y_2O_3 (SN1). Corrosion was monitored by mass change, eluate chemistry, microstructure of the penetrated zone and fracture strength. The main corrosion mechanism is the leaching of the grain boundary phases. The penetrated depths consists of at least two zones with an outer layer, which is characterised by a complete or at least extensive removal of the total grain boundary phase and an inner zone, where pure silica, from which Y and Al have been leached, persists. The rates of dissolution of Al, Y and Si ions decreased with corrosion time. The fracture strength decreased with increasing degree of dissolution of the grain boundary phase. Changes in the chemistry of the grain boundary phases result in strong changes of corrosion resistance. Successful corrosion penetration depth monitoring can be done by polarised reflected light optical microscopy (colour changes), Micro Raman Spectroscopy (luminescence changes) and SEM (porosity changes). The corrosion process and its kinetics are evidenced best by microanalysis of cross sections, Raman spectroscopy and the eluate chemistry changes in addition to mass changes.

Keywords: Corrosion; Fracture; Grain boundaries; Si_3N_4

1. Introduction

Silicon Nitride (Si_3N_4) ceramics are widely-used in engineering applications because of high fracture strength, high toughness, light weight, high temperature and corrosion resistance.[1] In the sintering additives such as MgO, Y_2O_3, Al_2O_3 are commonly used. The corrosion behaviour in various environments is a limiting factor for the life time of such ceramic components. Many corrosion tests have been conducted in environments such as hot gases, molten salts, metals or slags and often the corrosion resistance was shown to be good in these high temperature environments.[2–5]

For this reason the dangerousness of corrosion of Si_3N_4 under moderate conditions (< 200 °C) in aqueous solutions was underestimated for a long time. It was reported that Si_3N_4 ceramics without additives are very resistant to acids in various concentrations.[2,6,7] The presence of sintering additives changes the fluid corrosion behaviour, which depends on the chemical composition of the grain boundary phase and the degree of crystallization.[8] Significant corrosion was reported in hydrofluoric acid,[8] hydrochloric acid,[7] nitridic acid[9] and sulphuric acid.[10]

The monitoring of corrosion in aqueous solutions is usually performed by checking mass and/or strength change after immersion into a fixed volume of corrodent. In this study we have investigated the corrosion behaviour of two Yttria-Alumina/Magnesia-doped Si_3N_4 ceramics in a open system with a constant flow rate, i.e. under steady state conditions, and characterised the corrosion process with numerous analytical techniques.

2. Experimental procedure

Two cold isostatically pressed Si_3N_4 ceramics containing app. 6 wt.% Y_2O_3 and 4 wt.% Al_2O_3 (“SN0”) and 2,4 wt.% $MgAl_2O4$ and 1,3 wt.% Y_2O_3 (“SN1”) were used in the corrosion tests in diluted sulphuric acid. XRD investigations did not show any indication for crystalline phases within the grain boundaries.

* Corresponding author.
E-mail address: nickel@uni-tuebingen.de (K.G. Nickel).

0955-2219/03/$ - see front matter
PII: S0955-2219(02)00280-7

The samples were cut and ground into rectangular 3.5·3·45 mm beams. Fig. 1 illustrates the setup of the corrosion test apparatures consisting of teflon parts (PTFE) for the corrosion cell and tubes for pumping the fluid. The corrosion cell was constructed to spin up to 5 samples in the corroding agent (Fig. 1b).

A peristaltic pump was used to maintain a controllable and constant flow-rate during the time of the experiments. Already at a relatively slow flow rate of 0.24 ml/min (~145 l/100 h) the agent in the corrosion cell (30 ml) is replaced approximately every 2 h.

With an oil bath a temperature of 90 °C was kept with a precision of +/−1 °C. Thus the temperature was at least 10 °C below the boiling temperature of the diluted sulphuric acid.[10]

The preparation was as follows: the samples were washed in acetone for 10 min, rinsed with deionized water for 2 min, put into a cabinet dryer for at least 2 h at 150 °C, and weighed on a microbalance after a 2 h cooling period. After the experiment the samples were rinsed with deionized water, dried and weighed using the same procedures.

Further investigations were made with Raman spectroscopy, microprobe (EPMA), optical microscope, atomic absorbtion spectroscopy (AAS) and ICP-AES. 4-point-bending tests were conducted by standard procedures (DIN 51 110). However, the number of specimen tested after any single treatment was ⩽5, hence not sufficient for the requirements of obtaining secure statistical strength values.[11]

In intervals of several 10 h approximately 50 ml of eluate were taken to observe the leaching behaviour. The amounts of silicon, aluminium and yttrium were measured with the AAS and ICP–AES technique. The yttria concentrations in the eluats of SN1 could only be resolved using a ICP mass spectrometer (MS).

Microraman spectroscopic investigations were made with a Dilor LabRam apparatus and lasers of wavelengths 488, 532 and 632.8 nm. The highest lateral resolution of the laser beam has a spot diameter of app. 1 μm.

Microprobe (EPMA) measurements were performed on a Jeol-8900 superprobe in the wavelength dispersive mode (WDS).

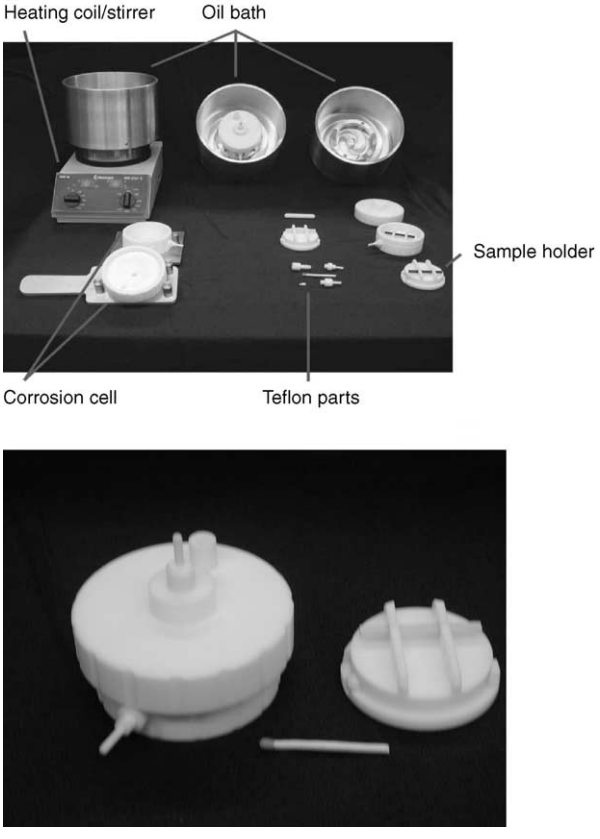

Fig. 1. Illustration of the apparatus for corrosion tests and the heating system, (a,top): overview (b,mid): illustration of the corrosion cell (PTFE).

3. Results

3.1. Mass loss

Fig. 2 shows the mass loss after 100 h treatment in acids of varying concentration. Material SN0 shows a 200 times higher mass loss than SN1, but both types of ceramics experience a higher mass loss by decreasing the molarity of the acid. Mass losses for SN0/SN1 after 211 h treatment in deonized water were about 16/22 μg/cm^2, which is close to the longtime stability limit of our balance. A mass losses after 100 h for $n=0$ in Fig. 2 would therefore be negligible.

This increase in mass loss with decreasing acid concentrations has been observed before with other acids as well.[7,8,12] An exception of this behaviour was reported only for HF-based aqueous solutions.[13] The feature is usually attributed to the higher solubility of species formed in the corrosion process in weaker acids. Alternatively an enhanced condensation reaction, re-establishing Si–O–Si bonds from dissolved Si–OH species in stronger acids may explain this feature as a passivation.

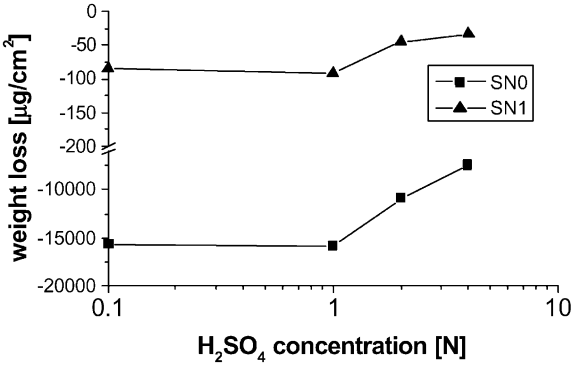

Fig. 2. Mass loss for SN0/1 of 100 h in various concentrations of diluted H_2SO_4 at 90 °C.

In a number of experiments with SN0 in 1n H_2SO_4 at 90 °C we used flow rates from 0.24 to 3 ml/min, hereby changing the time required for a complete exchange of the corroding medium in the chamber by a magnitude of order. We did not record a significant effect in relation to the variation of the flow rate.

Fig. 3 shows the mass change of SN0 (a) and SN1 (b) during corrosion tests in 1 N and 1 M H_2SO_4 as a function of exposure time. The strongest corrosive attack occurs in the first stage. After the first 24 h the mass loss is considerably slower.

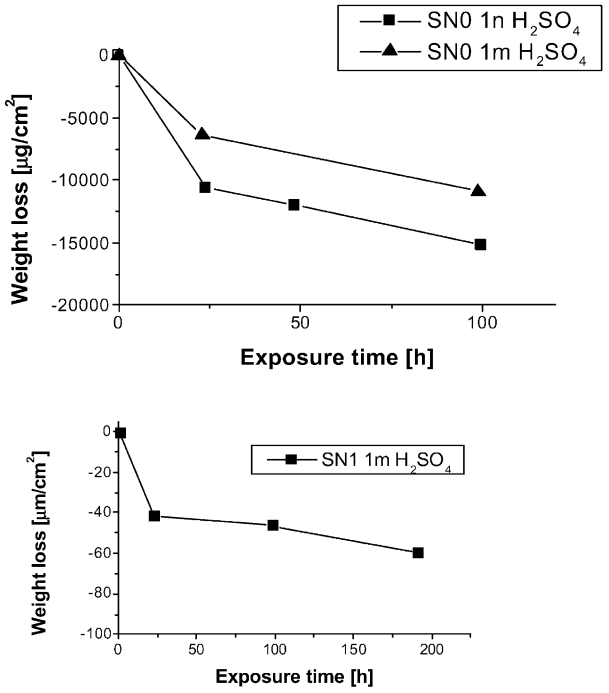

Fig. 3. Mass loss for SN1 (a, upper fig.) and SN0 (b, lower fig.) versus exposure time tested in 1 M and 1 N and 1 M H_2SO_4 at 90 °C, respectively.

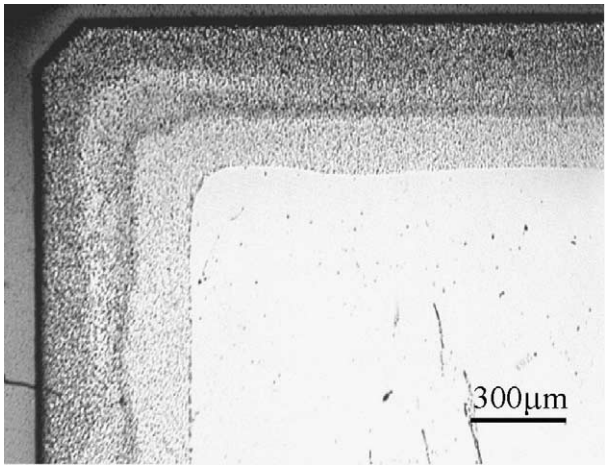

Fig. 4. Cross section of a corroded SN0 specimen, recorded with optical reflected light microscopy after 100 h in 1 M H_2SO_4.

3.2. Penetration

In order to find out, how mass change translates into corrosion penetration, we determined this value by a number of means.

Fig. 4 shows the cross section of a corroded SN0 specimen, recorded by optical microscopy in reflection

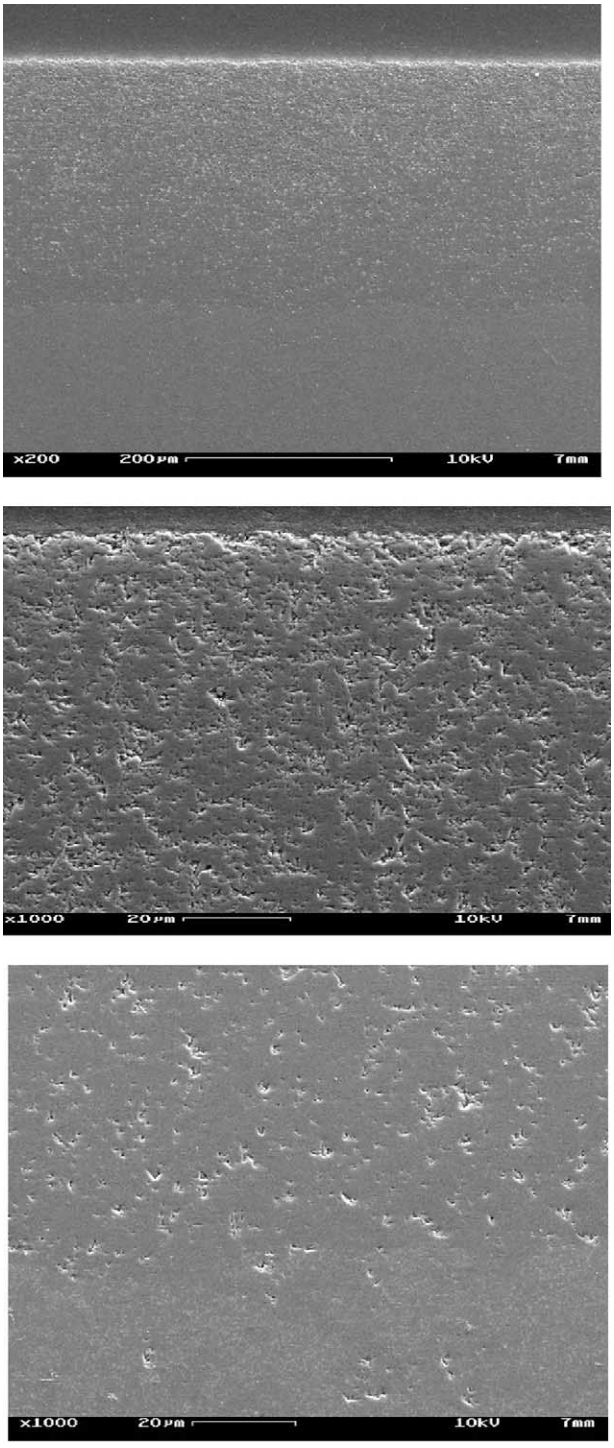

Fig. 5. Cross section of a corroded SN0 sample imaged by SEM after 23 h in 1 M H_2SO_4: (a, top): overview, (b, mid): outer porous zone, (c, bottom): lower porous zone.

mode. The region penetrated by corrosion is indicated by a number of colour changes from dark to bright grey. The boundary to the uncorroded bulk material is well defined and sharp at least to a level of a few microns.

Within the corrosion zone several subzones with different colours are visible in Fig. 4. Individual boundaries between such zones seem not to be as sharp as the one to the uncorroded zone, but the innermost zone with its change to darker grey levels is well defined.

SEM images of a cross section of a corroded SN0 specimen are shown in Fig. 5. Here we observe a porous zone, which is approximately 200 μm thick (Fig. 5a). Towards the sample surface there is a strong and uniform porosity (Fig. 5b), while the porosity decreases towards the corrosion front (Fig. 5c).

As an alternative way of checking the extent of the corrosion zone we have used Micro-Raman spectroscopy. In Fig. 6a and b Raman spectra of SN0 and SN1 before corrosion using a wavelength of 488 nm are shown. The Raman peaks can be attributed to Raman active modes for β-Si_3N_4 known from literature and theory.[14] In the spectrum of SN1 we find an additional peak at 522 cm^{-1}. It is attributed to free silicon in the bulk material. The presence of free silicon in silicon nitride ceramics and its colouring properties are known.[15]

In contrast to the well resolved spectra of the uncorroded material, Raman spectra from the corroded zone are widely dominated by luminescence, where only the peaks around 200 cm^{-1} are barely visible (Fig. 6c). In order to investigate the nature of this luminescence we have increased the investigated shift range to up to 9000 cm^{-1} (Fig. 6d). There are four major bands at 528, 565, 602 and 641 nm. These may be attributed to defect structures of SiO_2, because all modifications of silica are known to cause luminescence radiation in this region.[15]

It is possible to use the appearance of the luminescence to characterise the penetration of the corrosion front as shown in Fig. 7. The sublayers, which were identified by optical microscopy, have different levels of luminescence. It should be noted that there is a maximum close to the corrosion front, which drops off sharply.

3.3. The chemistry of the eluate

We have used a steady state approach in the corrosion experiments. This allows us to check the corrosion behaviour over time by monitoring the according changes of

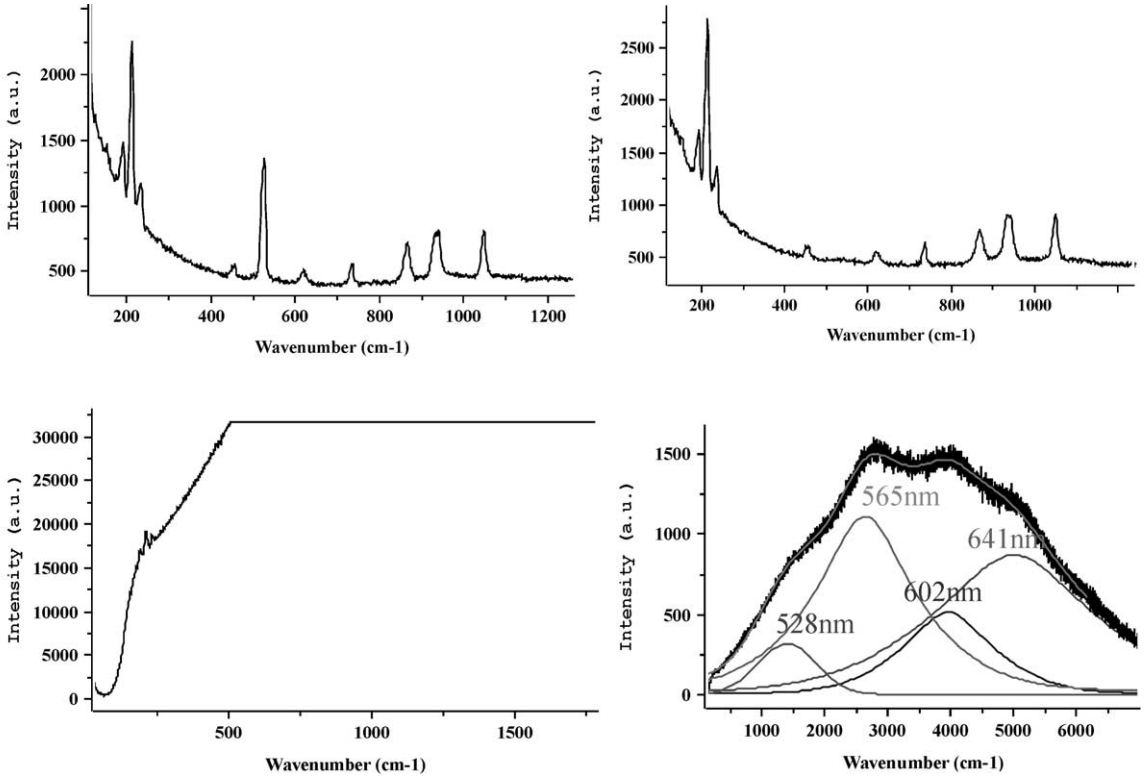

Fig. 6. Raman spectra (488 nm laser wavelength) of the uncorroded SN1 (a, top left) and SN0 (b, top right) and within the corrosion layer of SN0, showing strong luminescence (c, bottom left), with different ranges of peak shift (d, bottom right). The strong band at 520 cm^{-1} SN1 (a, top, left) can be attributed to free silicon.

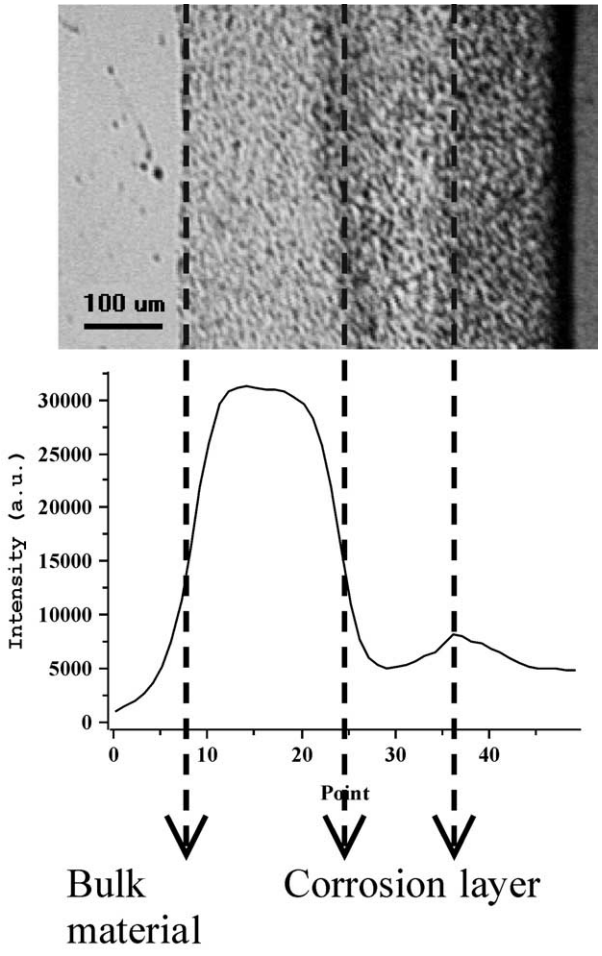

Fig. 7. Relative intensity of luminiscentic radiation in relation to the visible colour changes in the corrosion layer of SN0 (cp. Fig. 4).

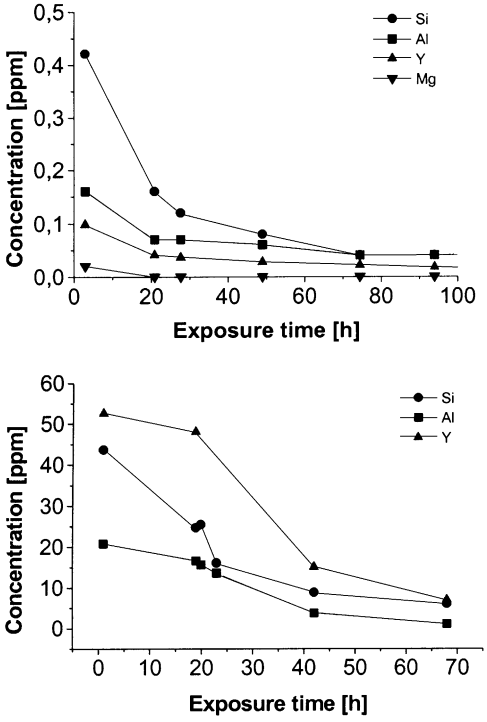

Fig. 8. Silicon, aluminium and yttrium concentrations in the eluate as a function of exposure time from corrosion tests in 1 M H_2SO_4 at 90 °C of SN1 (Fig. A, top) and 1 N H_2SO_4 at 90 °C of SN0 (Fig. B, bottom).

the element concentrations in the eluate with time. This is shown for SN0 and SN1 in Fig. 8.

The concentrations for SN1 are very small as expected from the corresponding low mass loss. While the absolute concentrations differ strongly there is a strong decrease in the eluate concentrations with time in both experiments and low concentration levels are approached for both specimen at long exposure times. In the SN1 specimen Al, Y and Mg seem to approach a stable concentration at very low levels already after app. 20 h, while the decrease in SN0 is over a much longer period. Only Si concentrations in eluate of SN0 seem to stay at relatively high levels.

3.4. The chemistry of the corroded zone

We have followed the chemical changes within the corroded layer of SN0 in Fig. 9 by WDS- linescans. This was only successful for material SN0, linescans in the SN1 material failed to show decreases of any elements within the lateral resolution.

The inner corrosion front in SN0 is characterised by a sharp step in the Y and Al concentrations, which vanish in the background level. Silicon and nitrogen show little change, because both zones are dominated by the presence of Si_3N_4. A interesting feature is the oxygen gradient within the corroded layer with oxygen dropping towards the outside of the specimen to a background level.

The depth of the boundary, where Y and Al vanish completely corresponds to the innermost corrosion front of Fig. 4, while the depth, at which the oxygen level drops below the detection limit correlates to the onset of the highly porous zone in Fig. 5. This inner less porous zone is obviously identical to the zone of high Raman luminescence seen in Fig. 7.

It is interesting to note that the two principal corrosion zones (1 = outer, highly porous zone without oxygen and 2 = inner zone with oxygen, but without Y and Al) can be monitored to grow with time in a constant ratio (Fig. 10).

3.5. Strength

Fig. 11 shows the mass loss and the 4-point-bending strength of SN0 as a function of penetration depth for specimen corroded by 1n H_2SO_4 at 90 °C. A linear relation between mass loss, penetration and strengths is indicated.

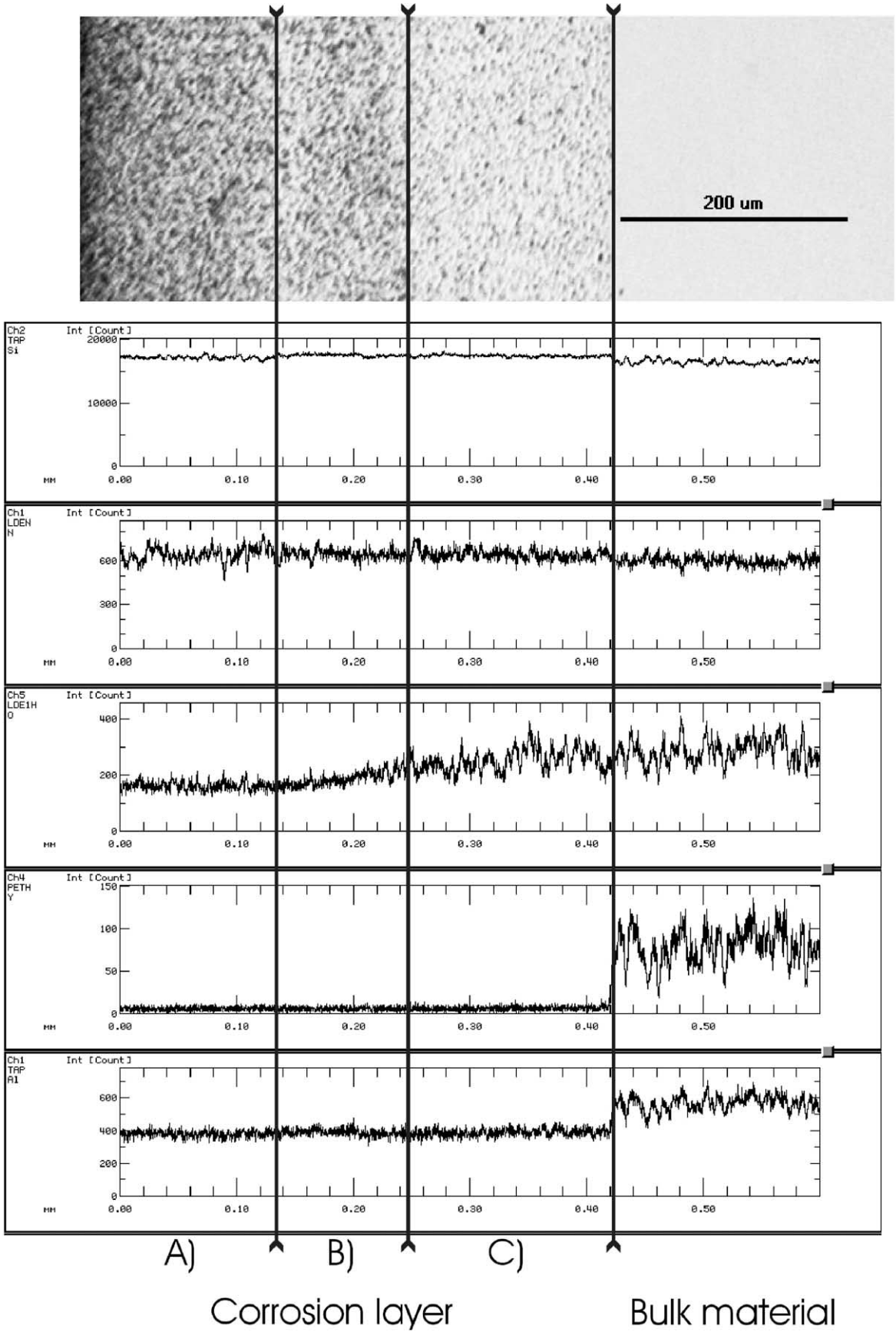

Fig. 9. WDS-linescan across the corrosion layer of SN0 in comparison with the optical micrograph (top). There are two principle corrosion zones: (A) without oxygen and (B),(C) with oxygen. Yttrium and aluminium are absent in the whole corrosion layer.

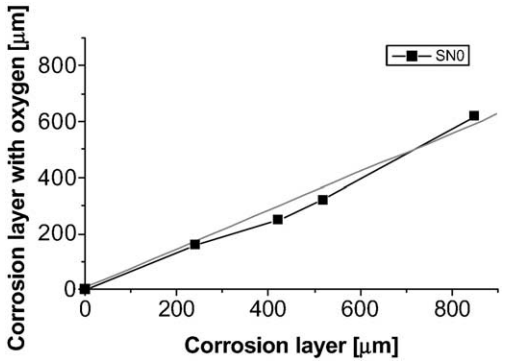

Fig. 10. Comparison of the extent of the zones of the corrosion layer, where yttria is absent but oxygen is still detectable (corrosion zone B),(C) in Fig. 9) versus the total corrosion depth in SN0 ceramic from several exposure times.

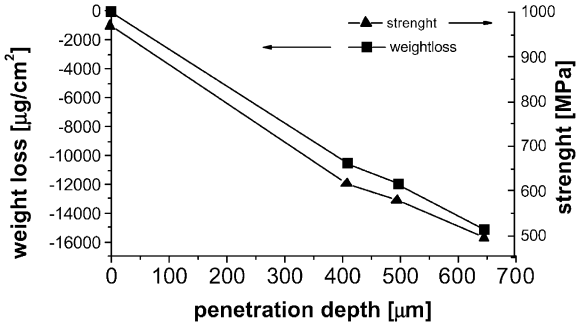

Fig. 11. Mass loss and 4-point-bending-strength versus penetration depth for SN0 corroded in 1 N H_2SO_4 at 90 °C.

4. Discussion

We have monitored the corrosion behaviour of sintered Si_3N_4 with several methods. All methods indicate the partial or complete removal of the grain boundary phase to be the main operating mechanism. A loss of material is already evidenced by checking the mass change of corroded samples. The chemistry of eluate recovered from different stages of the corrosion process reveals that all grain boundary constituents (Y, Al, Mg, Si, O) are subject to leaching in hot sulphuric acid.

We will discuss the details of the kinetics elsewhere but from the data from eluats it is clear that leaching of the glassy Y-Al-grainboundary phase is a differential process, which generally slows down with time. The chemistry changes of the corroded zone suggest an outer part with little or no silica left on top of a zone, where Y and Al have already been removed from a still existing silica. This layer of pure silica between silicon nitride grains is growing with time.

The presence of an inner silica layer is also evidenced by the luminescence recorded by Micro Raman spectroscopy, which suggests a high defect level in the silica. Accordingly the transport properties of this zone may not be identical to that of silica scales from oxidation processes. The low but definite luminescence in the outer corrosion zone adds evidence for silica removal but indicates remainders thereof, be it inside thin grain boundary films on silicon nitride grains or in triple points. The very presence of such remaining silica is also suggested by the lack of evidence for spallation.

The least costly method of penetration monitoring seems to be by reflected polarized light microscopy, which reveals all zones and indicates further differentiations within the corrosion layer, which are not yet clear.

SEM investigations will record the corrosion zone by the presence of voids from the removed triple point grain boundary phase. The decrease of porosity inwards the corrosion layer may be another indicator for a differentiated dissolution of the grain boundary phase.

From the good correlation of strength, mass change, chemistry and optical properties it is concluded that any of those are possible monitors for the penetration, which allow the extrapolation of the other properties once the—probably material depended—factors are known to convert the one to the other.

Finally the extremely low corrosion level for our material SN1 shows that it is possible to develop silicon nitride materials with extreme resistance to attack by sulphuric acid.

5. Conclusions

The penetration of two cold isostatic pressed Si_3N_4 Materials with different amounts of additives in diluted sulphuric acid was monitored. Both ceramics showed completely different corrosion characteristics in acidic aqueous solutions. Mass loss, penetration depth and strength measurements showed a good corrosion resistance of SN1 compared to SN0 for diluted sulphuric acids.

SEM indicated that SN0 was attacked primarily along the grain boundaries, especially the triple point boundary phases were dissolved. Conventional optical microscopy showed colour changes in the corrosion layer, which could be attributed to a change in the porosity and the presence of silica in the inner corrosion layer. Raman Spectroscopy is also a quick and easy method for the determination of penetration by detecting the high defect levels of remaining silica in the corrosion layer.

SN1 with the lower content of additives was attacked very slowly. Formation of a corrosion layer was not detectable. The role of magnesium in the grain boundary phase with respect to the corrosion resistance is not yet clear, but it is assumed that the lower additive content increases the silica content in the grain boundary phase and this improves the corrosion resistance of the glass phase.[16]

The shape of the mass loss curves, which was verified by AAS/ICP-AES analyses, indicated that the dissolution rate of the grain boundary phase rapidly decreases after corrosion times exceeding 24 h.

Acknowledgement

This work was supported by the Deutsche Forschungsgemeinschaft (DFG) under contract number Ni299/7.

References

1. Fletcher, A., *Silicon Nitride and the SIALONS*, Vol. 1. Elsevier Science publishers, 1993.
2. Lewis, L., *Corrosion Resistance of Technical Ceramics*. Her Majesty's Stationery Office, London, 1984.
3. Gogotsi, G. A., Zavada, V. P. and Gogotsi, Y. G., Strength degradation of Si_3N_4–SiC-based ceramics in salt enviroments. *Ceramics International*, 1986, **12**, 203–208.
4. Kim, H. E. and Moorhead, A. J., High-temperature gaseous corrosion of Si_3N_4 in H_2-H_2O and Ar-O_2-environments. *J. Am. Ceram. Soc*., 1990, **73**(10), 3007–3014.
5. Berthold, C., Degradation von Si3N4 als Ventilwerkstoff durch Oxidation und Salzschmelzkorrosion bei Einsatztemperaturen. Dissertation, Shaker Verlag, 1997.
6. Sangster R.S., *Si: Silicon Nitride: Chemical Reactions (continued)*. Springer-Verlag, 1995, Suppl. Vol. B 5d2.
7. Sato *et al*., Corrosion of silicon nitride ceramics in aqueous hydrogen chloride solutions. *J. Am. Ceram. Soc*., 1988, **71**(12), 1074–1079.
8. Sato *et al*., Corrosion of silicon nitride ceramics in aqueous HF solutions. *J. Mater. Sci*., 1988, **23**, 3440–3446.
9. Kanbara, K., Corrosion of silicon nitride ceramics by nitric acid. *Mater. Res. Soc. Proc*., 1993, **287**.
10. Okada, A., Corrosion behavior of silicon nitride ceramics in aqueous solutions (Part 2). *J. Ceram. Soc. Jap. Int. Edition*, 1992, **100**, 80–83.
11. Deutsches Institut f. Normung e.V., Testing of advanced technical ceramics, four bending test at room temperature. *DIN 51110,* 1990.
12. Okada, A. *et al*., Corrosion behavior of silicon nitride ceramics in aqueous solutions (Part 1). *J. Ceram. Soc. Jap. Int. Edition*, 1991, **99**, 1223–1227.
13. Sharkawy, S. W. and El-Aslabi, A. M., Corrosion of silicon nitride ceramics in aqeous HCl and HF solutions at 27–80 °C. *Corrosion Science*, 1998, **40**(7), 1119–1129.
14. Wada *et al*., Raman and IR absorbtion spectroscopic studies on α,β, and amorphous Si3N4. *J. Non-crystalline Solids*, 1981, **43**, 7–15.
15. Kalceff, M. A. S. and Phillips, M. R., Catholuminescence microcharacterization of the defect structure of quartz. *Physical Rev. B*, 1995, **52**(5), 3122–3134.
16. Herrmann, M., Schubert, Ch. and Micheal, G., Korrosionsverhalten keramischer Werkstoffe für Anwendungen in Wälzlagern und im Anlagenbau. *Fortschrittsberichte der Deutschen Keramischen Gesellschaft*, 1999, **14**(1).